mater.scichina.com link.springer.com

Published online 17 July 2020 | https://doi.org/10.1007/s40843-020-1379-4
Sci China Mater 2021, 64(1): 158–168

Facial synthesis of highly stable and bright $CsPbX_3$ (X=Cl, Br, I) perovskite nanocrystals *via* an anion exchange at the water-oil interface

Cong Fang[1], Ye Li[1], Yuting Cai[1], Tian-Liang Zhou[1], Xueyuan Tang[1,2*] and Rong-Jun Xie[1*]

ABSTRACT **Cesium lead halide perovskite nanocrystals (NCs) have attracted unprecedented attention owing to their compelling properties for optoelectronic applications. Compared with the classical hot-injection method, the room-temperature (RT) synthetic strategy is more facile and tender, but it is hard to obtain stable $CsPbI_3$ NCs and it usually uses polar solvents that sometimes reduce the stability and properties of NCs. Here, we reported a simple approach to synthesize highly efficient and stable $CsPbI_3$ as well as other color-tunable $CsPbX_3$ NCs with high quantum efficiency at room temperature *via* an anion exchange at the water-oil interface, in which the as-synthesized pristine $CsPbBr_3$ NCs in toluene were treated in aqueous solutions of HX (X=Cl, Br, and I) and protonated oleylamine (OAm) acted as a carrier. The synthesized $CsPbI_3$ NCs had an emission at 680 nm and even showed excellent colloidal stability after being stored for 32 d. The high efficiency and stability of the obtained $CsPbX_3$ NCs were ascribed to the facts that: (i) the polar reagents were almost removed from the surface of NCs; (ii) the defect-related nonradiative recombination was suppressed efficiently by surface passivation.**

Keywords: $CsPbX_3$, perovskite, nanocrystals, anion exchange, synthesis

INTRODUCTION

All inorganic cesium lead halide ($CsPbX_3$, X=Cl, Br, and I) perovskite nanocrystals (NCs) have recently attracted significant attention for their extraordinary optoelectronic properties [1–4], including high optical absorption coefficient, narrow full-width-at-half-maximum (FWHM), and tunable emissions covering the entire visible spectra [5–8]. Therefore, $CsPbX_3$ NCs are considered as the most promising materials for the next-generation optoelectronic devices, such as light-emitting diodes (LEDs), solar cells, and photodetectors [9,10].

To date, there are mainly two synthetic methods for $CsPbX_3$ NCs. One is the hot-injection reaction method that is commonly used to prepare $CsPbX_3$ NCs with high photoluminescence quantum yields (PLQYs), but it needs high temperature (140–200°C) and an inert atmosphere that result in high cost and limited output [11]. Another one is the room-temperature (RT) synthetic method enabling to facilely produce $CsPbBr_3$ NCs in a high yield without heating and stringent conditions [12–15]. However, the RT strategy is severely limited by using polar reagents (such as dimethyl sulfoxide (DMSO) or *N*,*N*-dimethylformamide (DMF)). These polar reagents, such as DMF, can reduce the stability and efficiency of NCs due to the inherent ionic characteristic of $CsPbX_3$ [16–18]. Typically, $CsPbI_3$ NCs synthesized at room temperature are easily degraded within a few days, making the RT method not suitable for $CsPbI_3$ NCs.

There are still some obvious drawbacks in the RT method *via* the anion-exchange reaction for $CsPbX_3$ NCs. First, the toxic benzoyl halides are often used to promote the substitution of the halide component in $CsPbX_3$ NCs [19,20]. Second, some reagents of the halide source, such as alkylammonium halides, will lead to the conversion of $CsPbBr_3$ NCs into Cs_4PbBr_6 and $CsPb_2Br_5$ NCs [21,22]. Third, the degradation of NCs sometimes occurs due to ultrasonic treatments and microwave irradiations that promote the complete exchange [23–25]. In addition, the post-synthesis processing, such as purification to remove excess reagents, can also decrease the PLQYs. Therefore, it is necessary to develop new RT synthetic routes to

[1] College of Materials, Xiamen University, Xiamen 361005, China
[2] Fujian Key Laboratory of Advanced Materials, Key Laboratory of High Performance Ceramic Fibers (Ministry of Education), Xiamen University, Xiamen 361005, China
* Corresponding authors (emails: xytang@xmu.edu.cn (Tang X); rjxie@xmu.edu.cn (Xie RJ))

synthesize highly stable $CsPbX_3$ NCs, without using DMF.

As we know, $CsPbX_3$ NCs are usually distributed in organic solvents, such as toluene and *n*-hexane. Organic solvents and water will form a water-oil interface owing to the difference in polarity. However, the polar reagents (i.e., DMF, DMSO) in NCs solutions tend to dissolve in water because their polarities are similar. Therefore, it is expected that the aqueous solution of HX (X=Cl, Br, I) can be used to remove the polar reagents at the water-oil surface. The aqueous solution of HX can also be employed as an active halide source to realize a high-quality anion exchange and obtain highly luminescent $CsPbX_3$ NCs at the water-oil surface. Furthermore, the water passivation and halogen-rich environment can improve the stability of $CsPbX_3$ NCs [17,26,27].

Herein, we report a facile method to synthesize full-color $CsPbX_3$ NCs by treating the pristine $CsPbBr_3$ NCs in the aqueous solution of HX (X=Cl, Br, I, 0.36% of HCl, 48% of HBr, 47% of HI) at room temperature. The polar reagents at the surface of $CsPbBr_3$ NCs can almost be removed at the water-oil interface owing to their similar polarity to the aqueous solution of HX. Simultaneously, the aqueous solution of HX is employed as the halide source to demonstrate successive and accurate adjustment of the maximum PL emission of $CsPbX_3$ NCs in the full visible spectral range (410–695 nm). The resultants, $CsPbCl_3$, $CsPbBr_3$ and $CsPbI_3$, show a high PLQY of 35%, 98% and 75%, respectively. The $CsPbI_3$ NCs have a PL emission at 680 nm and an FWHM of 44 nm, exhibiting an obviously enhanced colloidal stability. The mechanism of the post-synthetic interface engineering is investigated in $CsPbBr_3$ NCs. The proposed method is enabled to synthesize highly efficient and stable $CsPbX_3$ NCs (especially $CsPbI_3$ NCs) at room temperature.

EXPERIMENTAL SECTION

Materials

Lead(II) bromide ($PbBr_2$, 99%, Aladdin), cesium bromide (CsBr, 99.9%, Aladdin), butyric acid (BA, AR, Aladdin), oleylamine (OAm, 80%–90%, Aladdin), DMF (99.5%, Aladdin), toluene (99.5%, SCRC), HI (55.0%–58.0%, Aladdin), HBr (48%, Aladdin) and HCl (36.46%, SCRC) were purchased from commercial sources and used as received.

Preparation of oleylammonium bromide

Twenty-five milliliter of ethanol and 3.125 mL of OAm were mixed in a 250-mL flask and maintained at 0°C using ice water bath, then 4 mL of HBr was added slowly. After the ice water bath was removed, the mixture was kept for 3 h under the protection of N_2 gas. After that, the product was dried under vacuum to remove excess ethanol and washed with diethyl ether. The final product was collected after vacuum-drying at 80°C.

Synthesis of pristine $CsPbBr_3$ NCs

CsBr (0.1 mmol, 0.0212 g), and 0.2 mmol of $PbBr_2$ (0.0734 g) were dissolved in 5 mL of DMF absolutely *via* ultrasonication, and 80 μL of OAm and 150 μL BA were quickly injected to form a precursor solution by using a pipettor. The precursor solution (150 μL) was added to 5 mL of toluene under vigorous stirring. Finally, the bright $CsPbBr_3$ NC solution was obtained for various characterizations and the crude solution of $CsPbBr_3$ NCs was used for long-term storage.

Aqueous solution of HX treatment

Firstly, the aqueous solution of HCl was diluted and employed as the reaction reagents. One milliliter of HCl, HBr, or HI aqueous solution (0.36% of HCl, 48% of HBr, 47% of HI) was loaded in a glass bottle, and 2 mL of the as-prepared $CsPbBr_3$ NCs in toluene was dropped inside. Then the mixture was stored under ambient condition and the color changed from green to blue for the HCl aqueous solution or red for the HI aqueous solution. The NCs solution on the water-oil interface was collected through a pipette. Finally, the stable $CsPbX_3$ NCs solution was obtained. The final products were used for further analysis.

Characterization

X-ray diffraction (XRD) patterns were measured with a Bruker D8 Advance X-ray powder diffractometer equipped with Cu Kα radiation (λ=1.540 Å). The PL emission spectra of the samples were investigated by a Hitachi F4600 fluorescence spectrophotometer (Hitachi Co. Ltd., Japan) at room temperature. The ultraviolet-visible (UV-Vis) absorption spectra were recorded by using a spectrophotometer (UV-3600 PLUS, Shimadzu Co. Ltd., Japan). The absolute PLQYs were performed using an integrating sphere on an absolute PL quantum yield spectrometer C11347 (Hamamatsu, Japan) and the excitation wavelength was 400 nm at room temperature. The PL decay curves were collected at room temperature by using the FLS980 spectrometer equipped with a 445 and 375 nm pulse laser. The sizes and morphologies of the samples were obtained *via* a transmission electron microscope (JEOL, JEM-2100, Japan) operating at

200 kV. Fourier transform infrared (FTIR) spectra were obtained from 500 to 4000 cm^{-1} using a Thermo Scientific Nicolet iS10 FTIR spectrometer (Waltham, USA). The X-ray photoelectron spectroscopy (XPS, Ulvac-Phi, Inc., Japan) was measured to analyze the elemental composition. The transient absorption (TA) measurements were performed on a Helios pump-probe system (Ultrafast Systems LLC) equipped with an amplified femtosecond laser system (Coherent, 35 fs, 1 kHz, 800 nm) under ambient conditions. The pump pulses (375–650 nm) were obtained by focusing the 800 nm beam (split from the regenerative amplifier with a tiny portion, ~400 nJ per pulse) onto a sapphire plate. The 365 nm pump pulses (~2 μJ cm^{-2}) were obtained from an optical parametric amplifier (TOPAS-800-fs). The ^{1}H nuclear magnetic resonance (^{1}H NMR) spectra of the samples were collected using a Bruker Avance II 500 MHz NMR spectrometer (Switzerland) and the solvent was $CDCl_3$.

RESULTS AND DISCUSSION

The pristine $CsPbBr_3$ NCs, distributed in toluene, were synthesized *via* a traditional method (see the Experimental Section). The aqueous solution of HX (X=Cl, Br, I) was loaded in a glass bottle, and the $CsPbBr_3$ NC solution was dropped inside. Then, the toluene and aqueous solution of HX formed a water-oil interface. Bright $CsPbCl_3$ and $CsPbI_3$ NCs were obtained *via* an ion exchange. Simultaneously, DMF in toluene was penetrated into the aqueous solution through the water-oil interface. As shown in Fig. 1a, when the $CsPbBr_3$ NC solution is treated with the HI aqueous solution, a continuous red shift of the PL spectra is observed by controlling the reaction time (Video S1). Replacing HI by HCl results in a blue shift of the PL spectra (Video S2). With the increase of processing time, the continuous blue-shift from 518 to 410 nm and red-shift from 518 to 695 nm in emission spectra are observed, respectively (Fig. 1b). As seen in Fig. 1d, the XRD peaks gradually shift to small angles or to high angles with the halide changing from Br to I or from Br to Cl, which leads to the lattice shrinkage or expansion [28,29]. It should be noted that the maximum PL emission of the $CsPbBr_3$ NCs can be shifted to 695 nm or to 410 nm when they are treated in the HI or HCl aqueous

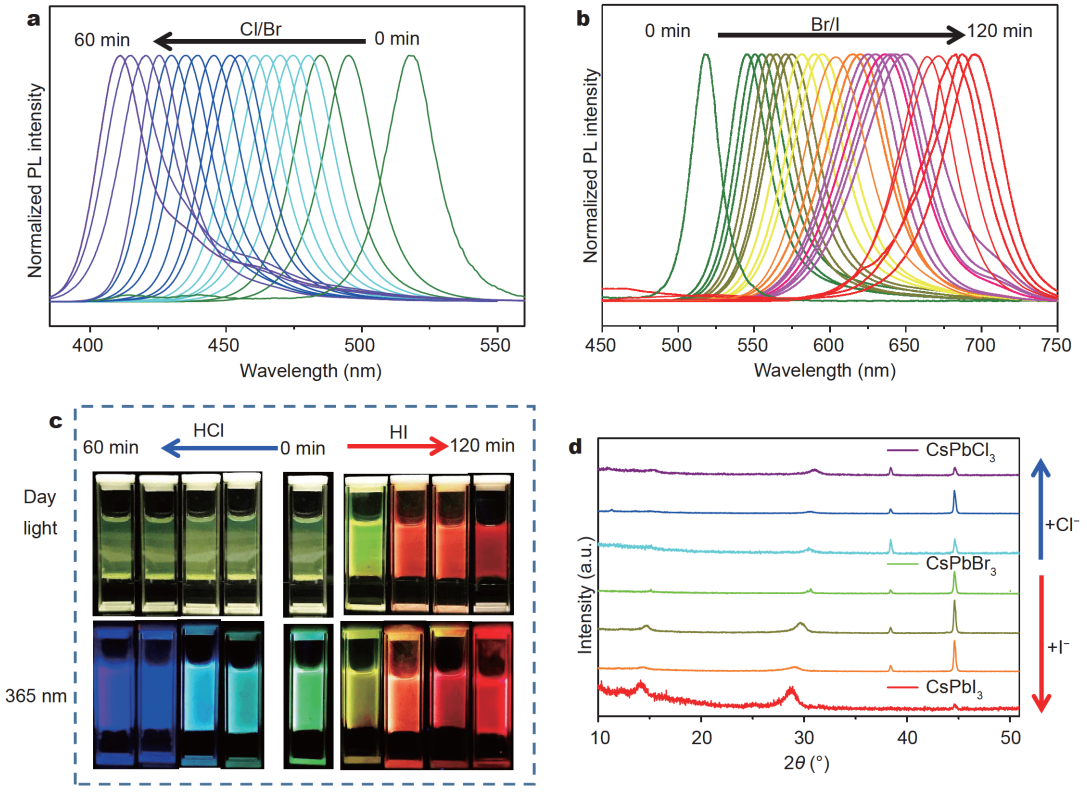

Figure 1 (a, b) PL spectra of the pristine $CsPbBr_3$ NCs and $CsPbX_3$ NCs treated with different aqueous solutions of HX for varying reaction times. Photos (c) and XRD (d) patterns of the pristine $CsPbBr_3$ NCs and $CsPbX_3$ (X=Cl, I) NCs prepared *via* the anion-exchange with different aqueous solutions of HX.

solution. Of course, the $CsPbBr_3$ NC solution can also be treated with the HBr aqueous solution. The pristine $CsPbBr_3$ NCs have a PL peak at 518 nm and a narrow FWHM of about 18 nm. The PL peak of the $CsPbBr_3$ NCs treated in the HBr aqueous solution is shifted to 512 nm (Fig. S1). No obvious change is seen in the maximum PL emission, but the treated $CsPbBr_3$ NCs show improved photoluminescence. The synthesized $CsPbCl_3$, $CsPbBr_3$ and $CsPbI_3$ show a high PLQY of 35%, 98% and 75%, respectively. In addition, the PLQYs are higher than that of the $CsPbX_3$ NCs obtained *via* the anion-exchange method in the recent report ($CsPbCl_3$, $CsPbBr_3$ and $CsPbI_3$ NCs possessed a PLQY of 32.4%, 90.2% and 62.7%, respectively) [23]. Compared with the classical $CsPbX_3$ NCs prepared at room temperature, the new $CsPbX_3$ NCs present a wider wavelength range (410–695 nm) with higher PLQYs (Table S1). The results indicate that the proposed method is facile and enabled to complete the ion exchange at the water-oil interface totally and to increase the PL properties of $CsPbX_3$ NCs.

The transmission electron microscopy (TEM) images and high-resolution TEM (HRTEM) images of the pristine $CsPbBr_3$ NCs and HX-treated $CsPbX_3$ NCs are shown in Fig. 2. All NCs show a cubic morphology. The size of the pristine $CsPbBr_3$ NCs is 12.6±1.3 nm (Fig. 2a, e). After being treated with the HBr or HCl aqueous solution, the size of the NCs decreases from 12.6 to 8.2 nm or to 8.7 nm (Fig. 2b, c). However, the synthesized $CsPbI_3$ NCs have a particle size of 14 nm. Notably, the amount of black dots adhered to the pristine $CsPbBr_3$ NCs decreases after the treatment. It has been reported that the black dots are metallic Pb [27,30,31], which may originate from the decomposition of $CsPbX_3$ NCs by DMF. The result indicates the amount of DMF is greatly reduced by the treatment. Furthermore, the XRD patterns verify that the treated $CsPbBr_3$ and $CsPbCl_3$ NCs possess orthorhombic and tetragonal structures, respectively (Fig. S2a, b).

The stability of the $CsPbI_3$ NCs was investigated by monitoring their PLQYs and PL intensities. After being stored under ambient and dark conditions for 32 d, the $CsPbI_3$ NCs show only a little change of color, while they still have bright red emission under UV light irradiation (Fig. 3a). As seen in Fig. 3b, the $CsPbI_3$ NCs have a cubic structure and the structure remains unchanged after 32 d of storage. The red $CsPbI_3$ NCs exhibit the maximum PL emission at 680 nm and an FWHM of 44 nm (Fig. 3c). No obvious changes of shape and peak position are observed in the PL spectra after 32 d. As shown in Fig. 3d, the PLQY of $CsPbI_3$ NCs remains high at ca. 70%, and only shows a very small decline as the storage time increases up to 32 d. These results confirm the successful preparation of stable $CsPbI_3$ NCs at room temperature.

The stability of the obtained $CsPbBr_3$ NCs was also evaluated. As shown in Fig. 4a, the pristine $CsPbBr_3$ NC solution has undergone an obvious color change and aggregation after 30 d. However, the treated $CsPbBr_3$ NC solution shows no obvious change in color and still has bright emission under UV light irradiation. In Fig. 4b, one can find that the PLQY of the pristine $CsPbBr_3$ NCs

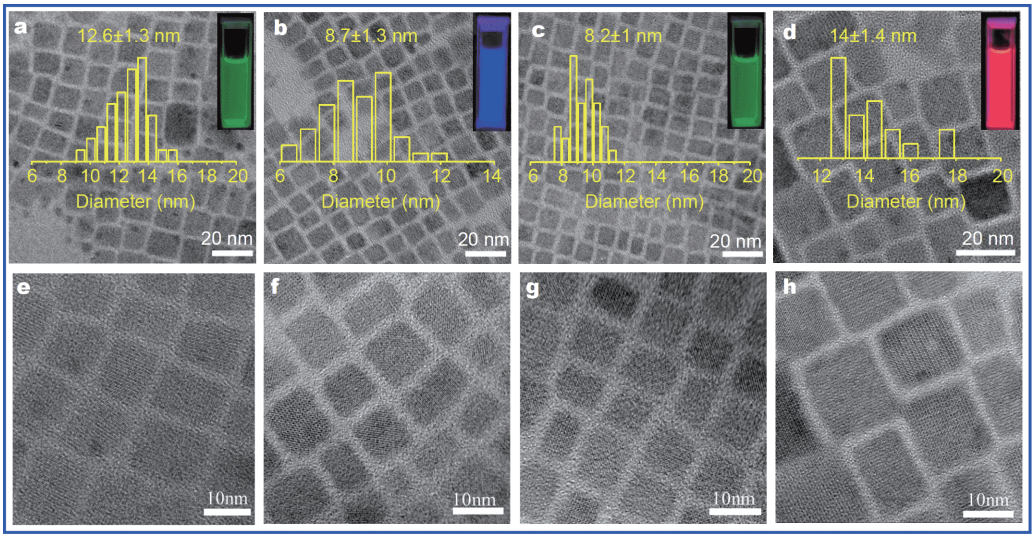

Figure 2 TEM and HRTEM images of the pristine $CsPbBr_3$ NCs (a, e), $CsPbCl_3$ NCs (b, f), $CsPbBr_3$ NCs (c, g) and $CsPbI_3$ NCs (d, h) prepared by treating the pristine $CsPbBr_3$ NCs with different aqueous solutions of HCl, HBr and HI, respectively.

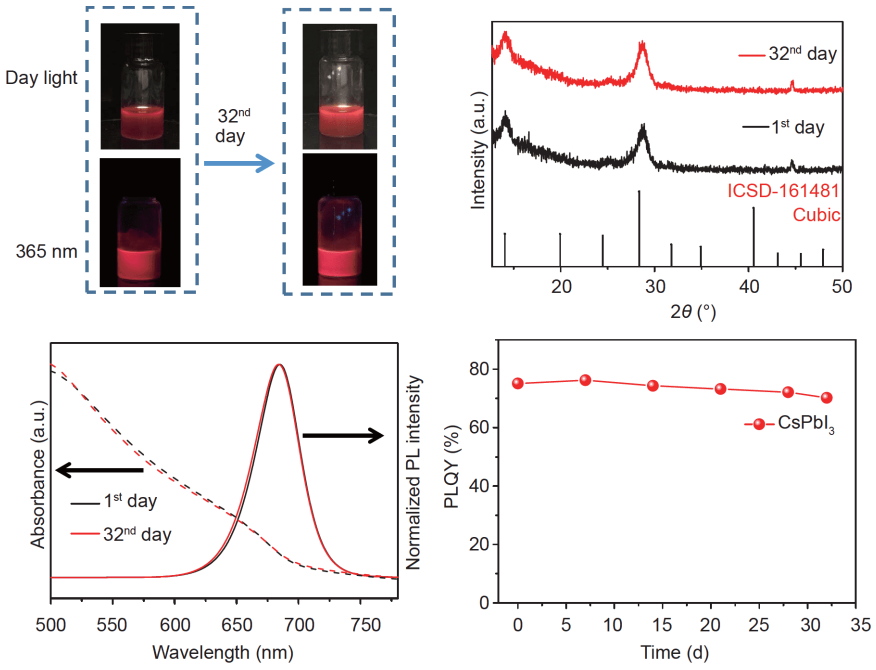

Figure 3 (a) Photograph comparisons of the $CsPbI_3$ NCs before and after 32-d storage, in daylight (up) and under UV light (bottom), respectively. XRD patterns (b), absorbance and PL spectra (c) and PLQYs (d) of the $CsPbI_3$ NCs as a function of storage time.

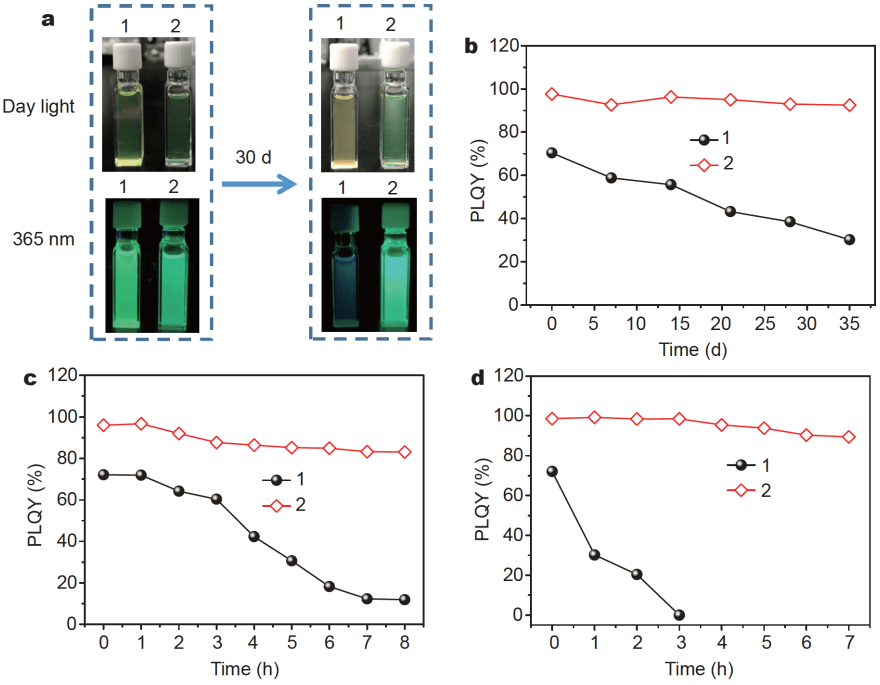

Figure 4 (a) Photographs of the pristine $CsPbBr_3$ NCs (1) and treated $CsPbBr_3$ NCs (2) in daylight and under UV light (left), and those of the corresponding $CsPbBr_3$ NCs after 30 d. (b) PLQYs of the pristine (1) and treated (2) $CsPbBr_3$ NC solutions in toluene. (c) PLQYs of the pristine (1) and treated (2) $CsPbBr_3$ NCs under UV light irradiation. (d) PLQYs of the pristine (1) and treated (2) $CsPbBr_3$ NCs in the saturated humidity at 25°C.

decreases quickly from 71% to 30% after exposure in ambient atmosphere for 35 d, while the treated $CsPbBr_3$ NCs can maintain 92% PLQY and only lose 6% of PLQY. In addition, as seen in Fig. 4c, the treated NCs dispersed

in toluene have a PLQY of 83% after 8 h UV light (365 nm, 6 W) irradiation, but the PLQY of the pristine NCs dispersed in toluene decreases to 11%. We also estimated the water stability of these NCs in a saturated humidity at 25°C (Fig. 4d). The relative PLQY of the treated $CsPbBr_3$ NCs dispersed in toluene remains 90% of the initial intensity after 7 h and nearly keeps constant within a longer time, which is much higher than that of the pristine $CsPbBr_3$ NCs dispersed in toluene (declines to zero in 3 h). It indicates that the treated $CsPbBr_3$ NCs have a much better water resistance. The improved stability and PLQY could be attributed to the surface passivation after the treatment in the aqueous solution of HBr [17,27,32].

As we know, the decline in PLQY can be attributed to the nonradiative pathway of surface defects [27,33–36]. The PL lifetimes of all samples were then measured to investigate the surface changes after treatment. As shown in Fig. 5a, the PL decay curve of the pristine $CsPbBr_3$ NCs is multi exponential in nature. According to previous reports, the long-lifetime is ascribed to shallow surface defects [26,27,37]. As the treatment time increases, the lifetime becomes shorter (Fig. S3 and Table S2). It could originate from the removal of shallow surface defects and the reduction in proportion of the long-lifetime component. Simultaneously, the PL decay curve finally becomes single-exponential after the treatment. Similar results are observed in the $CsPbCl_3$ and $CsPbI_3$ NCs (Fig. S4). The PL lifetimes (τ_{ave}) are 10.56 and 50 ns, which are close to that of the highly luminescent NCs reported elsewhere [23,38]. In addition, the PL decay curve of $CsPbI_3$ also becomes single-exponential after the treatment (Fig. S4b). The change of the PL decay curves further indicates that the pristine product exhibits a defect-related nonradiative recombination and the passivation strategy eliminates the nonradiative recombination pathways effectively. Furthermore, the XPS analyses of the pristine and treated $CsPbBr_3$ NCs were performed to confirm the surface change. We know that Pb atoms in the NCs are assumed to have two chemical environments, one is in a higher binding energy (BE) region for Pb–Br and another is in a lower BE region for Pb-oleate [39]. The slightly increased binding energy of the Pb 4f peak indicates that the number of the Pb–Br species increases in the treated $CsPbBr_3$ NCs compared with the pristine $CsPbBr_3$ NCs, as shown in Fig. 5b [40]. Simultaneously, according to the quantitative XPS results, the Pb:Br ratio changes after the treatment (Fig. S5b). The pristine sample has a Pb:Br ratio of 1:2.97, implying a Pb-rich surface. After the treatment, the Pb:Br ratio increases to 1:3.3, which is an

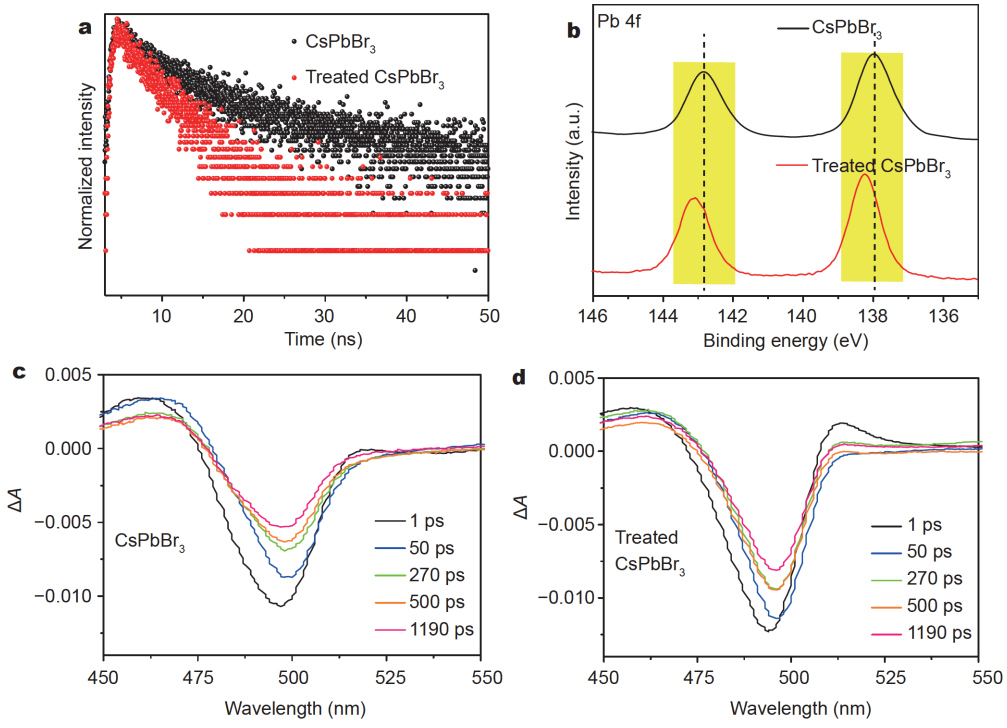

Figure 5 (a) PL decay curves of the pristine and treated $CsPbBr_3$ NCs. (b) XPS spectra corresponding to Pb 4f of the pristine and treated $CsPbBr_3$ NCs. TA spectra of the (c) pristine and (d) treated $CsPbBr_3$ NCs.

indicative of a Br-rich surface environment [39]. The results indicate that surface halogen defects contributing to the nonradiative recombination are reduced after the treatment [41,42]. The transient absorption (TA) spectra were measured to further reveal the exciton densities of the pristine and treated $CsPbBr_3$ NCs. All TA spectra show an identical bleach signal at around 490 nm with a pump intensity of 2 μJ cm^{-2} (Fig. 5c, d). As we know, ΔA is proportional to the exciton density at the lowest excited state in NCs [43,44], and an obvious difference can be seen in the TA spectra (Fig. 5a, b, and Figs S6 and S7). ΔA decreases fast between 1 and 1190 ps for the pristine $CsPbBr_3$ NCs, whereas it decreases slowly and maintains high intensity at 1190 ps for the treated $CsPbBr_3$ NCs. The higher signal intensity indicates that excitons are more easily transited to the valence band in the treated NCs and are less likely to be trapped by surface defects after being passivated by the aqueous solution of HX. These results explain why the treated $CsPbX_3$ NCs have high PLQYs.

Another important reason for the performance improvement is the reduction in DMF. $CsPbX_3$ NCs can be dissolved by DMF due to the ionic characteristic [11]. As shown in the ^{1}H NMR spectra, resonances a′, b′ and c′ of DMF are found in the pristine $CsPbBr_3$ NCs, while they are not seen in the treated $CsPbX_3$ NCs (Fig. 6a). Though the content of DMF is very small in the pristine $CsPbBr_3$ NCs, the result also suggests that the amount of DMF can be reduced effectively by the treatment. The NCs were characterized by using FTIR spectroscopy (Fig. 6b). The peaks at 2920 and 2854 cm^{-1} come from BA and OAm, which can be assigned to the C–H stretching vibrations [45]. Peaks at 1584 cm^{-1} can be assigned to the N–H bending vibration, a characteristic band for OAm [46]. Compared with the pristine NCs, the treated NCs show stronger peaks of ligands. It indicates that the loss of ligand is suppressed and the surface of the NCs is passivated by the treatment [39,47,28].

In the anion-exchange method reported before, it is hard to accurately control the amount of halide ions. Therefore, it is often necessary to remove excess reagents and reaction byproducts by purification, which can cause some degradation of NCs [48]. Moreover, some extra energies commonly used for the halide exchange, such as photon irradiation, ultrasonic treatment, and microwave irradiation, may also cause the decomposition of NCs [49–52]. In our proposed approach, however, we can not only decrease the content of DMF, but also skip the purification step without introducing impurities for anion exchanges of $CsPbX_3$ NCs at the water-oil interface. As shown in Fig. 7, the pristine $CsPbBr_3$ NCs can be dispersed in toluene, and the green solution turns red from bottom to top gradually when the toluene solution is mixed with the aqueous solution of HI in a glass bottle. The ligand binding to the surface of NCs is highly dynamic, which thus indicates that the oleylammonium bromide does not tightly adhere to the NCs surface and the exchange between its bound and free states can happen [48,53,54], leading to the facile proton transfer of OAm surface capping reagents. Firstly, the I^- ions in the HI aqueous solution exchange with the Br^- ions in the $CsPbBr_3$ solution at the water-oil interface. The protonated OAm, acting as carriers, combines with I^-. When the free OAm returns to the surface of the NCs, the exchange from $Br^- \rightarrow I^-$ then happens. With increasing the processing time, the I^- ions will almost replace the Br^- ions. In this process, not only DMF is reduced effectively, but also no extra reagents like metal cations are left [23].

In order to verify the above mechanism and the effect of the protonated OAm in the process, we designed a series of control experiments. The pristine $CsPbBr_3$ NCs were dispersed in toluene, and then a small amount of HI

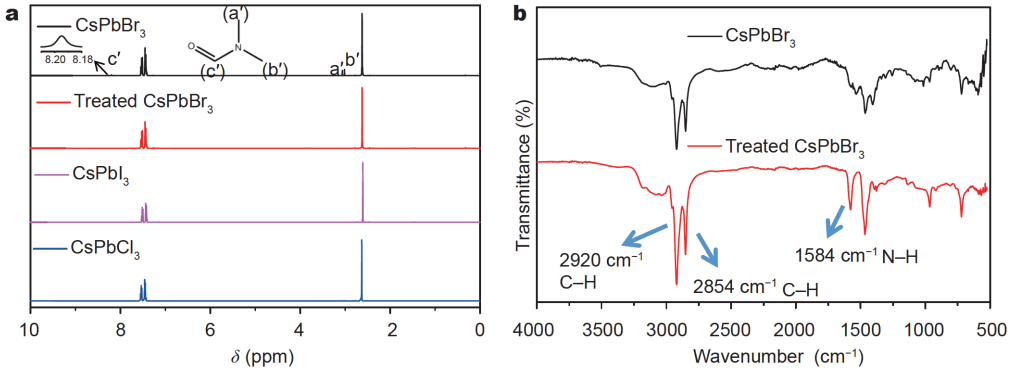

Figure 6 (a) ^{1}H NMR spectra of the pristine $CsPbBr_3$ NCs; treated $CsPbBr_3$ NCs, $CsPbI_3$ NCs and $CsPbCl_3$ NCs. (b) FTIR spectra of the pristine and treated $CsPbBr_3$ NCs.

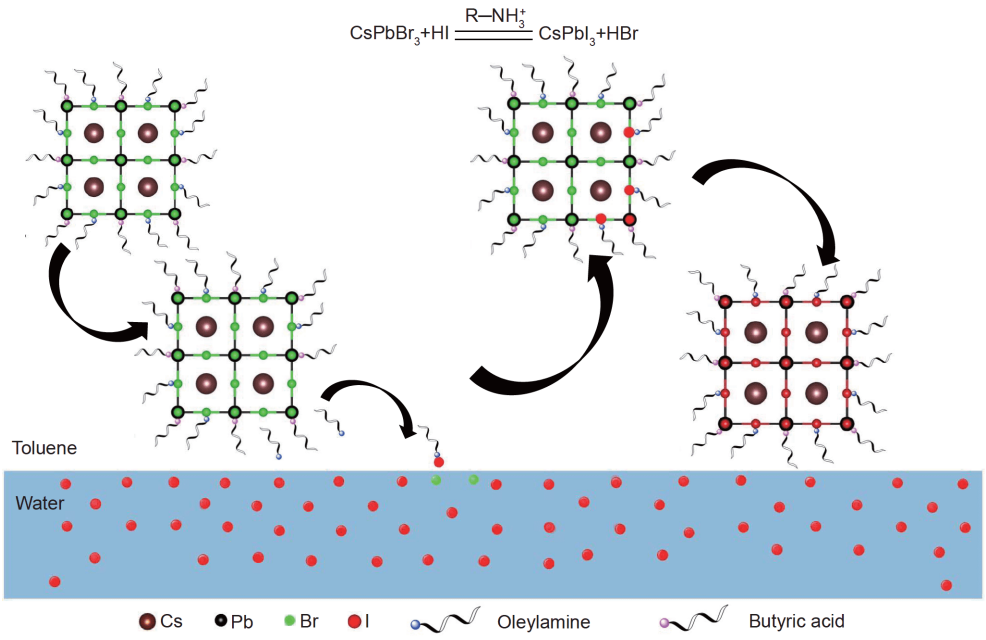

Figure 7 Schematic illustrations of the anion exchange at the water-oil interface.

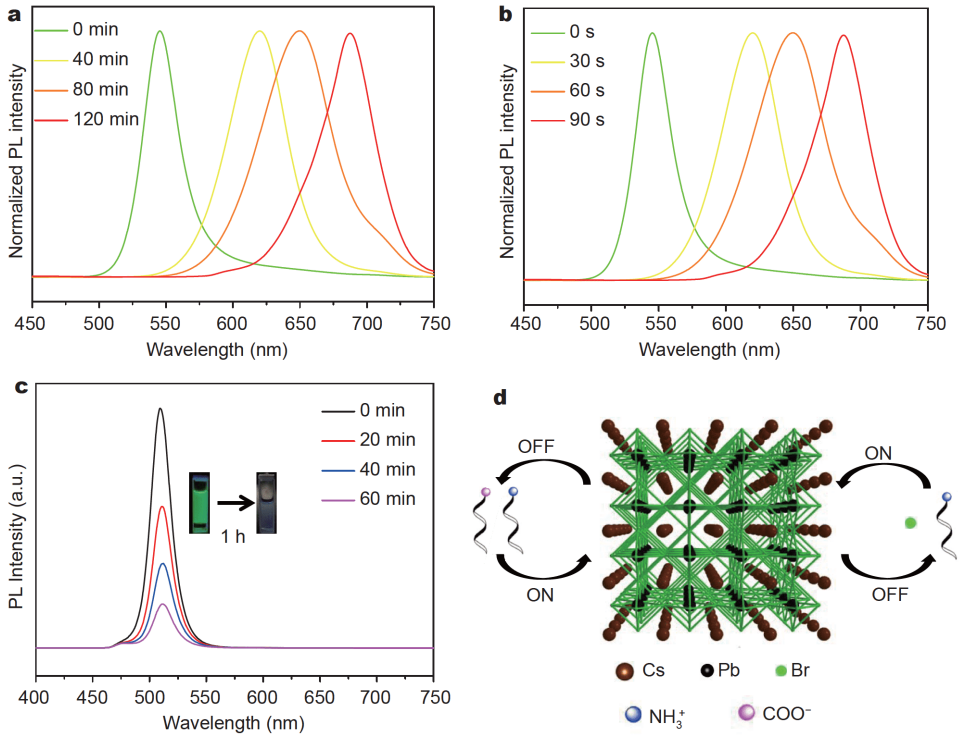

Figure 8 PL spectra of (a) the pristine $CsPbBr_3$ NCs with the HI aqueous solution, (b) the pristine $CsPbBr_3$ NCs treated in the aqueous solution of HI with extra oleylammonium bromide, and (c) the amine-free $CsPbBr_3$ NCs treated in the HI aqueous solution. (d) Schematic illustration of the dynamic surface stabilization.

aqueous solution was added for the anion exchange. It can be observed that the emission peak gradually red shifts to 680 nm till the shift stops in 2 h (Fig. 8a). For comparison, we prepared $CsPbBr_3$ NCs under the same

conditions expect for adding extra 10 mmol of oleylammonium bromide (Video S3). Obviously, the red shift can be completed only in a few minutes (Fig. 8b). To further confirm the key role of the protonated OAm, we performed a typical amine-free method to synthesize $CsPbBr_3$ by capping them solely using oleic acid (OA) for the anion exchange in the HI aqueous solution (Fig. 8c) [55]. The emission peak does not shift and the intensity shows a sharp decline because of the poor water stability of $CsPbBr_3$. Therefore, it can be concluded that the anion exchange of the OA-capped $CsPbBr_3$ NCs does not occur without the protonated OAm.

CONCLUSIONS

In summary, we successfully prepared highly efficient, stable and color-tunable $CsPbX_3$ NCs *via* an anion exchange at the water-oil interface, by treating the pristine $CsPbBr_3$ NCs in the aqueous solutions of HX (X=Cl, Br, and I) at room temperature. In the anion exchange process, the protonated OAm played a key role as carrier. Using this method, highly stable and efficient red $CsPbI_3$ NCs can be synthesized at room temperature, of which the PLQY is 75% and it remains almost unchanged after being stored in toluene for 32 d. The improved stability and PLQY of $CsPbX_3$ NCs can be attributed to the reduction of DMF on the surface of NCs and the surface passivation after the anion exchange.

Received 27 March 2020; accepted 3 May 2020; published online 17 July 2020

1 Gao X, Cui Y, Levenson RM, *et al. In vivo* cancer targeting and imaging with semiconductor quantum dots. Nat Biotechnol, 2004, 22: 969–976
2 Dai X, Zhang Z, Jin Y, *et al.* Solution-processed, high-performance light-emitting diodes based on quantum dots. Nature, 2014, 515: 96–99
3 Sheng X, Chen G, Wang C, *et al.* Polarized optoelectronics of $CsPbX_3$ (X=Cl, Br, I) perovskite nanoplates with tunable size and thickness. Adv Funct Mater, 2018, 28: 1800283
4 Zhai W, Lin J, Li Q, *et al.* Solvothermal synthesis of ultrathin cesium lead halide perovskite nanoplatelets with tunable lateral sizes and their reversible transformation into Cs_4PbBr_6 nanocrystals. Chem Mater, 2018, 30: 3714–3721
5 Wu Y, Wei C, Li X, *et al. In situ* passivation of $PbBr_6^{4-}$ octahedra toward blue luminescent $CsPbBr_3$ nanoplatelets with near 100% absolute quantum yield. ACS Energy Lett, 2018, 3: 2030–2037
6 Bekenstein Y, Koscher BA, Eaton SW, *et al.* Highly luminescent colloidal nanoplates of perovskite cesium lead halide and their oriented assemblies. J Am Chem Soc, 2015, 137: 16008–16011
7 Wang C, Zhang Y, Wang A, *et al.* Controlled synthesis of composition tunable formamidinium cesium double cation lead halide perovskite nanowires and nanosheets with improved stability. Chem Mater, 2017, 29: 2157–2166
8 Swarnkar A, Chulliyil R, Ravi VK, *et al.* Colloidal $CsPbBr_3$ perovskite nanocrystals: luminescence beyond traditional quantum dots. Angew Chem Int Ed, 2015, 54: 15424–15428
9 Protesescu L, Yakunin S, Bodnarchuk MI, *et al.* Nanocrystals of cesium lead halide perovskites ($CsPbX_3$, X=Cl, Br, and I): novel optoelectronic materials showing bright emission with wide color gamut. Nano Lett, 2015, 15: 3692–3696
10 Yang H, Zhang Y, Pan J, *et al.* Room-temperature engineering of all-inorganic perovskite nanocrsytals with different dimensionalities. Chem Mater, 2017, 29: 8978–8982
11 Wei S, Yang Y, Kang X, *et al.* Room-temperature and gram-scale synthesis of $CsPbX_3$ (X=Cl, Br, I) perovskite nanocrystals with 50%–85% photoluminescence quantum yields. Chem Commun, 2016, 52: 7265–7268
12 Li X, Wu Y, Zhang S, *et al.* $CsPbX_3$ quantum dots for lighting and displays: room-temperature synthesis, photoluminescence superiorities, underlying origins and white light-emitting diodes. Adv Funct Mater, 2016, 26: 2435–2445
13 Akkerman QA, Gandini M, di Stasio F, *et al.* Strongly emissive perovskite nanocrystal inks for high-voltage solar cells. Nat Energy, 2017, 2: 16194
14 Sun S, Yuan D, Xu Y, *et al.* Ligand-mediated synthesis of shape-controlled cesium lead halide perovskite nanocrystals *via* reprecipitation process at room temperature. ACS Nano, 2016, 10: 3648–3657
15 Veldhuis SA, Ng YF, Ahmad R, *et al.* Crown ethers enable room-temperature synthesis of $CsPbBr_3$ quantum dots for light-emitting diodes. ACS Energy Lett, 2018, 3: 526–531
16 Tong Y, Ehrat F, Vanderlinden W, *et al.* Dilution-induced formation of hybrid perovskite nanoplatelets. ACS Nano, 2016, 10: 10936–10944
17 Xie M, Liu H, Chun F, *et al.* Aqueous phase exfoliating quasi-2D $CsPbBr_3$ nanosheets with ultrahigh intrinsic water stability. Small, 2019, 15: 1901994
18 Di Stasio F, Christodoulou S, Huo N, *et al.* Near-unity photoluminescence quantum yield in $CsPbBr_3$ nanocrystal solid-state films *via* postsynthesis treatment with lead bromide. Chem Mater, 2017, 29: 7663–7667
19 Creutz SE, Crites EN, De Siena MC, *et al.* Anion exchange in cesium lead halide perovskite nanocrystals and thin films using trimethylsilyl halide reagents. Chem Mater, 2018, 30: 4887–4891
20 Imran M, Caligiuri V, Wang M, *et al.* Benzoyl halides as alternative precursors for the colloidal synthesis of lead-based halide perovskite nanocrystals. J Am Chem Soc, 2018, 140: 2656–2664
21 Balakrishnan SK, Kamat PV. Ligand assisted transformation of cubic $CsPbBr_3$ nanocrystals into two-dimensional $CsPb_2Br_5$ nanosheets. Chem Mater, 2018, 30: 74–78
22 Udayabhaskararao T, Houben L, Cohen H, *et al.* A mechanistic study of phase transformation in perovskite nanocrystals driven by ligand passivation. Chem Mater, 2018, 30: 84–93
23 Liu H, Liu Z, Xu W, *et al.* Engineering the photoluminescence of $CsPbX_3$ (X=Cl, Br, and I) perovskite nanocrystals across the full visible spectra with the interval of 1 nm. ACS Appl Mater Interfaces, 2019, 11: 14256–14265
24 Ruan L, Lin J, Shen W, *et al.* Ligand-mediated synthesis of compositionally related cesium lead halide $CsPb_2X_5$ nanowires with improved stability. Nanoscale, 2018, 10: 7658–7665
25 Ramasamy P, Lim DH, Kim B, *et al.* All-inorganic cesium lead halide perovskite nanocrystals for photodetector applications. Chem Commun, 2016, 52: 2067–2070

26 Liu P, Chen W, Wang W, *et al.* Halide-rich synthesized cesium lead bromide perovskite nanocrystals for light-emitting diodes with improved performance. Chem Mater, 2017, 29: 5168–5173
27 Li F, Liu Y, Wang H, *et al.* Postsynthetic surface trap removal of $CsPbX_3$ (X=Cl, Br, or I) quantum dots *via* a ZnX_2/hexane solution toward an enhanced luminescence quantum yield. Chem Mater, 2018, 30: 8546–8554
28 Tong Y, Bladt E, Aygüler MF, *et al.* Highly luminescent cesium lead halide perovskite nanocrystals with tunable composition and thickness by ultrasonication. Angew Chem Int Ed, 2016, 55: 13887–13892
29 Zhong H, Bai Z, Zou B. Tuning the luminescence properties of colloidal I-III-VI semiconductor nanocrystals for optoelectronics and biotechnology applications. J Phys Chem Lett, 2012, 3: 3167–3175
30 Udayabhaskararao T, Kazes M, Houben L, *et al.* Nucleation, growth, and structural transformations of perovskite nanocrystals. Chem Mater, 2017, 29: 1302–1308
31 Zhang M, Li H, Jing Q, *et al.* Atomic characterization of byproduct nanoparticles on cesium lead halide nanocrystals using high-resolution scanning transmission electron microscopy. Crystals, 2018, 8: 2
32 Gomez L, de Weerd C, Hueso JL, *et al.* Color-stable water-dispersed cesium lead halide perovskite nanocrystals. Nanoscale, 2017, 9: 631–636
33 Kang J, Wang LW. High defect tolerance in lead halide perovskite $CsPbBr_3$. J Phys Chem Lett, 2017, 8: 489–493
34 Liu Y, Xiao H, Goddard William A. I. Two-dimensional halide perovskites: tuning electronic activities of defects. Nano Lett, 2016, 16: 3335–3340
35 Pan J, Sarmah SP, Murali B, *et al.* Air-stable surface-passivated perovskite quantum dots for ultra-robust, single- and two-photon-induced amplified spontaneous emission. J Phys Chem Lett, 2015, 6: 5027–5033
36 Kim Y, Yassitepe E, Voznyy O, *et al.* Efficient luminescence from perovskite quantum dot solids. ACS Appl Mater Interfaces, 2015, 7: 25007–25013
37 Koscher BA, Swabeck JK, Bronstein ND, *et al.* Essentially trap-free $CsPbBr_3$ colloidal nanocrystals by postsynthetic thiocyanate surface treatment. J Am Chem Soc, 2017, 139: 6566–6569
38 Cai Y, Wang H, Li Y, *et al.* Trimethylsilyl iodine-mediated synthesis of highly bright red-emitting $CsPbI_3$ perovskite quantum dots with significantly improved stability. Chem Mater, 2019, 31: 881–889
39 De Roo J, Ibáñez M, Geiregat P, *et al.* Highly dynamic ligand binding and light absorption coefficient of cesium lead bromide perovskite nanocrystals. ACS Nano, 2016, 10: 2071–2081
40 Song J, Fang T, Li J, *et al.* Organic-inorganic hybrid passivation enables perovskite QLEDs with an EQE of 16.48%. Adv Mater, 2018, 30: 1805409
41 Manser JS, Christians JA, Kamat PV. Intriguing optoelectronic properties of metal halide perovskites. Chem Rev, 2016, 116: 12956–13008
42 Wang Y, Lü X, Yang W, *et al.* Pressure-induced phase transformation, reversible amorphization, and anomalous visible light response in organolead bromide perovskite. J Am Chem Soc, 2015, 137: 11144–11149
43 Zhao Y, Li J, Dong Y, *et al.* Synthesis of colloidal halide perovskite quantum dots/nanocrystals: progresses and advances. Isr J Chem, 2019, 59: 649–660
44 Zhang Y, Ding C, Wu G, *et al.* Air stable PbSe colloidal quantum dot heterojunction solar cells: ligand-dependent exciton dissociation, recombination, photovoltaic property, and stability. J Phys Chem C, 2016, 120: 28509–28518
45 Kumawat NK, Swarnkar A, Nag A, *et al.* Ligand engineering to improve the luminance efficiency of $CsPbBr_3$ nanocrystal based light-emitting diodes. J Phys Chem C, 2018, 122: 13767–13773
46 Zhong Q, Cao M, Hu H, *et al.* One-pot synthesis of highly stable $CsPbBr_3@SiO_2$ core-shell nanoparticles. ACS Nano, 2018, 12: 8579–8587
47 Gao Y, Peng X. Photogenerated excitons in plain core CdSe nanocrystals with unity radiative decay in single channel: the effects of surface and ligands. J Am Chem Soc, 2015, 137: 4230–4235
48 Nedelcu G, Protesescu L, Yakunin S, *et al.* Fast anion-exchange in highly luminescent nanocrystals of cesium lead halide perovskites ($CsPbX_3$, X=Cl, Br, I). Nano Lett, 2015, 15: 5635–5640
49 Parobek D, Dong Y, Qiao T, *et al.* Photoinduced anion exchange in cesium lead halide perovskite nanocrystals. J Am Chem Soc, 2017, 139: 4358–4361
50 Jang DM, Kim DH, Park K, *et al.* Ultrasound synthesis of lead halide perovskite nanocrystals. J Mater Chem C, 2016, 4: 10625–10629
51 Long Z, Ren H, Sun J, *et al.* High-throughput and tunable synthesis of colloidal $CsPbX_3$ perovskite nanocrystals in a heterogeneous system by microwave irradiation. Chem Commun, 2017, 53: 9914–9917
52 Li H, Brescia R, Povia M, *et al.* Synthesis of uniform disk-shaped copper telluride nanocrystals and cation exchange to cadmium telluride quantum disks with stable red emission. J Am Chem Soc, 2013, 135: 12270–12278
53 Hens Z, Martins JC. A solution NMR toolbox for characterizing the surface chemistry of colloidal nanocrystals. Chem Mater, 2013, 25: 1211–1221
54 Akkerman QA, D'Innocenzo V, Accornero S, *et al.* Tuning the optical properties of cesium lead halide perovskite nanocrystals by anion exchange reactions. J Am Chem Soc, 2015, 137: 10276–10281
55 Yassitepe E, Yang Z, Voznyy O, *et al.* Amine-free synthesis of cesium lead halide perovskite quantum dots for efficient light-emitting diodes. Adv Funct Mater, 2016, 26: 8757–8763

Acknowledgements This work was supported by the Natural Science Foundation of Fujian Province (2019J05041), the Education Foundation of Fujian Province (JAT170021), and the "Double-First Class" Foundation of Materials and Intelligent Manufacturing Discipline of Xiamen University.

Author contributions Tang X and Xie RJ conceived and designed the experiments; Fang C and Cai Y performed the experiments; Fang C and Li Y analyzed the data; Zhou TL contributed the materials tools; Fang C and Xie RJ wrote the paper.

Conflict of interest The authors declare that they have no conflict of interest.

Supplementary Information Supporting data are available in the online version of the paper.

Cong Fang is currently a graduate student at the College of Materials, Xiamen University. He obtained his bachelor degree from Fujian University of Technology in 2017. His current research focuses on the synthesis of perovskite nanocrystals.

Rong-Jun Xie received his PhD degree from Shanghai Institute of Ceramics, Chinese Academy of Sciences in 1998. He was Science and Technology Agency (STA) research fellow at the National Institute for Research in Inorganic Materials (Japan, 1998–2000), and Japan Science and Technology Agency (JST) research fellow at the National Institute of Advanced Industrial Science and Technology (Japan, 2001–2002) and Alexander von Humboldt research fellow at Darmstadt University of Technology (Germany, 2002–2003). He joined the National Institute for Materials Science (Japan) as Senior Researcher (2003–2007), Principal Researcher (2007–2014) and Chief Researcher (2014–2017). Since 2018, he has been a full professor in the College of Materials, Xiamen University (China). His research interests include the syntheses and applications of luminescent materials (phosphors, quantum dots (QDs), metal-organic frameworks (MOFs)), solid state lighting and other optoelectronic devices

基于水-油界面反应的离子交换法合成高效稳定的$CsPbX_3$ (X=Cl, Br, I)纳米晶

方聪[1], 李烨[1], 蔡宇廷[1], 周天亮[1], 唐学原[1,2*], 解荣军[1*]

摘要 全无机$CsPbX_3$钙钛矿纳米晶因其卓越的发光性能而在光电领域引起了前所未有的关注. 相对于传统的热注射法, 室温法是一种更简单、温和的合成钙钛矿纳米晶的方法. 然而, 在室温下很难获得稳定的$CsPbI_3$纳米晶, 并且室温法通常会使用极性溶剂, 这些溶剂有时会降低钙钛矿纳米晶的稳定性和性能. 本文提出了一种简单的合成方法, 通过在水-油界面处的阴离子交换, 在室温下合成了高效稳定的$CsPbI_3$纳米晶以及其他$CsPbX_3$纳米晶. 在合成过程中, 质子化的油胺充当载体. 测试分析结果表明: 所合成的$CsPbI_3$纳米晶的发射峰位于680 nm, 且在保存32天后仍然具有极好的发光稳定性. 所合成的$CsPbX_3$纳米晶的高量子效率和稳定性可归因于: (i) 极性试剂几乎从纳米晶溶液中去除; (ii) 通过表面钝化有效地抑制了与缺陷有关的非辐射复合.